Sedimentation-Diffusion Behaviour of Nanoparticles

francesco giorgi (francesco.giorgi@liverpool.ac.uk)
University of Liverpool https://orcid.org/0000-0002-7550-4217
Peter Macko
European Commission Joint Research Centre Ispra Sector
Judith M. Curran
University of Liverpool
Maurice Whelan
European Commission Joint Research Centre Ispra Sector
Andrew Worth
European Commission Joint Research Centre Ispra Sector
Eann A. Patterson
University of Liverpool

Research

Keywords: Gold nanoparticles, sedimentation–diffusion equilibrium, settling dynamics, gravitational sedimentation, target dose

Posted Date: May 7th, 2020

DOI: https://doi.org/10.21203/rs.3.rs-25349/v1

Sedimentation-diffusion behaviour of nanoparticles

Francesco Giorgi[1], Peter Macko[2], Judith M. Curran[1], Maurice Whelan[2], Andrew Worth[2], and Eann A. Patterson[1].

[1] Faculty of Science and Engineering, University of Liverpool, Liverpool L69 3GH, United Kingdom

[2] European Commission, Joint Research Centre (JRC), Ispra 21027, Italy

Abstract

Background: The biological response of organisms exposed to nanoparticles is often studied in vitro using adherent monolayers of cultured cells. In order to derive accurate concentration-response relationships, it is important to determine the local concentration of nanoparticles to which the cells are actually exposed rather than the nominal concentration of nanoparticles in the cell-culture medium. In this study, we investigated the sedimentation–diffusion process of different sized and charged gold nanoparticles in vitro by evaluating their settling dynamics and by developing a theoretical model to predict the concentration depth-profile of nanoparticles in solution over time.

Results: Experiments were carried out in water and in cell-culture media at a range of controlled temperatures. The optical phenomenon of caustics was exploited to track nanoparticles in real-time in a conventional optical microscope without any requirement for fluorescent labelling that potentially affects the dynamics of the nanoparticles. The results obtained demonstrate that size, temperature, and the stability of the nanoparticles play a pivotal role in regulating settling dynamics of nanoparticles. For gold nanoparticles larger than 60 nm in diameter, the initial nominal concentration did not accurately represent the concentration of nanoparticles local to the cells.

Conclusion: Nanoparticles dynamics in solution regulate the amount of material at the cellular level and must be taken into account when evaluating the biological response of organisms. the theoretical model proposed in this study accurately described the settling dynamics of the nanoparticles and thus represents a promising tool to support the design of in vitro experiments and the study of concentration-response relationships.

Keywords: Gold nanoparticles, sedimentation–diffusion equilibrium, settling dynamics, gravitational sedimentation, target dose.

Background

A dose–response assessment describes the response of an organism as a function of exposure to an exogenous agent. In the pharmaceutical sector for example, dose-response analysis is essential to estimate the dose at which a drug can have a therapeutic or adverse effect in patients [1]. One of the main principles of the dose-response paradigm is that the elicited biological response is proportional to the concentration of an administered agent at the site of action [2]. Thus, knowing the concentration within the target organ, tissue or cell population is a prerequisite for accurate dose-response modelling. However, measuring the local concentration at the site of action is not always practicably possible and thus often the initial administered concentration is used, which can lead to inaccuracies in determining dose-response relationships [3].

Gold nanoparticles are of great interest for a number of biomedical applications since they are a promising carrier for the targeted delivery of therapeutic, diagnostic and imaging agents in the human body [4]. They are also being explored as a means to subject stem cells to mechanical stimuli to activate certain signalling pathways and to modulate their differentiation [5]. As with small molecule agents, nanoparticle concentration has been reported as one of the primary factors determining positive as well as adverse effects on the biological organisms tested [6, 7].

In vitro studies of nanoparticles typically involve exposing a monolayer of cultured cells that are adhered to the bottom of a well in a microtiter plate. Frequently investigators use the nominal concentration of nanoparticles in the cell medium as a basis to determine dose-response relationships without taking into account that the concentration may not in fact be homogeneous in the well over time. This is due to the fact that nanoparticles in solution are subjected to gravitational sedimentation forces, Brownian diffusion forces and inter-particle forces which affect the transport of nanoparticles within the medium. This in turn controls the concentration of nanoparticles local to the cells that can influence cellular uptake [8, 9]. Therefore, a sufficient understanding of nanoparticle dynamics and distribution in solution is needed to more accurately determine concentration-response relationship in vitro.

Sedimentation – diffusion equilibrium

Nanoparticles dispersed in solution tend to sediment, diffuse and aggregate as a function of intrinsic properties (size, mass, surface charge, etc.) and as a function of system properties (viscosity, temperature, etc.). Once injected in solution, the process dominating the dynamics of nanoparticles is the diffusion process and nanoparticles tend to move from zones of high concentration to zones of low concentration of particles (Fig. 1a). After a certain time, an unstable equilibrium is achieved and nanoparticles are randomly but homogenously distributed in the medium (Fig. 1b). Gravitational sedimentation starts to occur in the homogeneous suspension for particles with a diameter bigger than 10 nm causing a concentration gradient from the bottom to the top of the solution [10]. This concentration gradient causes the diffusion flux of the particles to be contrary to their sedimentation flux. When the diffusion flux equals the sedimentation flux, a so-called sedimentation–diffusion equilibrium is achieved (Fig. 1c) [11]. The time at which this equilibrium is reached is called the settling time. Most studies described in the literature attempt to experimentally investigate the sedimentation–diffusion equilibrium process by acquiring UV-visible absorption spectra over time in an attempt to determine the behaviour of the nanoparticles in solution [12-14]. UV-visible spectroscopy is a powerful technique mainly used to analyse the colloidal stability of nanoparticle suspensions. The absorbance peak of the UV spectrum is related to the concentration of monodispersed particles in solution [15]. This technique has been used to investigate the sedimentation process by evaluating the decrease in concentration of monodispersed nanoparticles in solution over time. However, the detection limit of the spectrophotometer makes it impossible to perform analysis at low concentrations of particles [16]. Moreover, aggregates of particles can float in solution for a certain time depending on their size and the depth at which they were formed [17]. Finally, uncertainty in the acquired UV-visible spectra has been reported for solutions exhibiting a high gradient of nanoparticle concentration from the bottom to the top of the acquisition zone [13]. In this study, we investigated the sedimentation–diffusion process and evaluated the settling time of gold nanoparticles in a range of simple and biological solutions. Nanoparticles were tracked by exploiting the optical phenomenon of caustics and the nanoparticle concentration profile has been directly evaluated by acquiring consecutive optical sections from the bottom to the top of the solution and counting the number of particles in each section over time.

Investigators have also developed theoretical models to predict the observed sedimentation-diffusion behaviour of nanoparticles in solution [18]. The most common theoretical model used to describe the

concentration profile of nanoparticles in solution is the well-known Mason–Weaver equation, which combines the sedimentation and diffusion processes to predict the density of a solute at a certain depth in a solution [19]. The parameters of the Mason–Weaver equation are the diffusion coefficient and the sedimentation velocity calculated using the Stokes-Einstein diffusion equation and the Stokes sedimentation law, respectively. The Mason–Weaver model is based on the assumption that there are no interactions between nanoparticles and that their motion is only governed by random Brownian forces and a directional gravitational force [20]. However, the assumption of non-interacting particles can be valid only for a system with a very low particle concentration. Moreover, the Stokes–Einstein diffusion equation and Stokes sedimentation law can fail when predicting the dynamic behaviour of particles at the nanoscale because they do not take into account factors which have been reported to be dominant at the nanoscale, such as electrostatic and Van der Waals forces [21]. Several studies have already demonstrated that, depending on the properties of the nanoparticles and solution, the experimental diffusion and sedimentation coefficients differ from theoretical ones at the nanoscale [22 - 24].

In this study we investigated the settling dynamics of different sized gold nanoparticles in water and cell culture medium at a range of different temperature exploiting the optical phenomenon of caustics [25]. The comparison between experimental data and theoretical predictions of the Mason–Weaver equation confirmed that the current theoretical framework based on the Stokes-Einstein diffusion and Stokes sedimentation equations is not able to accurately describe the real dynamics of nanoparticles settling in a solution. Here, we propose a modified version of the Mason–Weaver equation (the Giorgi-Macko model) able to better predict the experimental concentration depth-profile of nanoparticles, by making the diffusion coefficient a function of the local concentration of nanoparticles, which is a factor that has been reported to influence the dynamics of nanoparticles in solution [23].

Results and discussion

Effect of size on nanoparticle sedimentation–diffusion equilibrium

The effect of nanoparticle size on the equilibrium of the sedimentation–diffusion process is shown in figure 2. The estimated concentration of settled nanoparticles and the relative settling time change as a function of the size of the nanoparticles. Larger particles tend to reach equilibrium faster with a higher concentration of particles transported to the bottom of the solution, but all the particles tested

exhibit a non-negligible deviation between the administered dose and the target dose at the equilibrium. Consider, for example the smallest size tested, approximately 50% of the 60 nm nanoparticles in solution settle migrating towards the bottom of the solution, meaning that the target dose is at least 1.5x the initial administered dose.

The reliability of classical Mason–Weaver equation in describing the concentration profile of the nanoparticles in solution over time has been assessed by plotting the concentration of not-settled nanoparticles along with the Mason-Weaver predictions (Fig. 3a). As expected, the Mason–Weaver equation, with the Stokes-Einstein diffusion coefficient and Stokes sedimentation velocity, is not able to predict the experimental results. The theoretical upward diffusion flux, which opposes the downward sedimentation flux of nanoparticles, is higher than the experimental one, leading to an overestimation of the concentration of the nanoparticles not settled once equilibrium is attained. The main factor affecting the diffusion flux in the Mason–Weaver equation is the diffusion coefficient evaluated using the Stokes–Einstein equation. Coglitore et al. [23] found by tracking single monodispersed nanoparticles that, below a critical size and concentration, the diffusion coefficient of the nanoparticles was at least one order of magnitude smaller than the theoretical value predicted by Stokes–Einstein equation and was independent of nanoparticle size.

Another limitation of the model is the assumption that the sedimentation velocity and diffusion coefficient exhibited by the particles in solution is constant with time, without taking into account that the concentration gradient formed once equilibrium is achieved can directly affect the sedimentation and diffusion behaviour of the nanoparticles. Ganguly et al. [26] demonstrated that the sedimentation velocity decreases as a function of the concentration because of the increased magnitude of the hydrodynamic interactions between particles. Kourki and Famili [27] observed the same decreasing trend of sedimentation velocity when investigating the sedimentation of silica nanoparticles. Coglitore et al. [23] explained the low values of diffusion coefficient obtained from experiments by considering that, at low concentrations, nanoparticle motion is almost entirely controlled by collisions with fluid molecules and the particle-particle interaction can be neglected. Koening et al. [28] reported a higher diffusion coefficient (of the same order of magnitude as the Stokes–Einstein prediction) using the same nanoparticles and solution but with a higher particle concentration. Considering this evidence, it is reasonable to conclude that the concentration of nanoparticles directly affects their diffusion and sedimentation behaviour through particle-particle interactions. In our test scenario, at the beginning of

the experiment nanoparticles are homogeneously monodispersed at low concentrations, so that particle-particle interactions are negligible and do not affect the sedimentation velocity while the diffusion coefficient is smaller than the theoretical one and mainly regulated by the fluid molecules. Once a concentration gradient forms in the solution, particle interactions start to influence the dynamics of the nanoparticles above the settling zone, leading to a decrease in sedimentation velocity and an increase in diffusion coefficient.

The Giorgi–Macko theoretical model has been developed to overcome the limitations of the classical Mason–Weaver equation, taking into account the experimental evidence and physical hypotheses discussed above. The distinctive feature of the model proposed in this study is the dependence of the diffusion coefficient on the local concentration of the nanoparticles (Eq. 6). The diffusion coefficient for each particle size tested has been set equal to the experimental value of $5x10^{-13}$ m^2 s^{-1} as reported in previous studies for gold nanoparticles at low concentrations [21, 23] and then progressively increased as function of the local concentration of nanoparticles to the values calculated using the Stoke–Einstein equation (Fig. S-2 in the Electronic Supplementary Material). As shown in figure 6b, this revised model predicts the experimental data more accurately than the classical Mason–Weaver model and can be used to estimate the settling dynamics over time of the nanoparticles and their concentration profile in solution. The deviations between the Giorgi–Macko model and the experimental data can be explained by the fact that the sedimentation velocity in the model has been kept constant at a value that gives the best fit for each size of nanoparticle tested and did not vary with their concentration, in order to reduce the mathematical complexity and computational requirements of the model (Fig. S-3 in the supplementary material).

The role of colloidal stability on nanoparticle sedimentation–diffusion equilibrium

The effect of temperature on the sedimentation–diffusion equilibrium was evaluated by testing 100 nm diameter negatively-charged gold nanoparticles in water at 23 °C and at the biologically-relevant temperature of 37 °C (Fig. 7a). The results obtained demonstrate that at 37 °C the sedimentation velocity increased and that the solution reached the sedimentation–diffusion equilibrium 30 minutes before the same solution at 23°C. The higher temperature directly influences the aggregation kinetics of gold nanoparticles, enhancing their aggregation rate in solution [29]. The UV-Visible spectra of the solutions kept at constant temperatures of 23°C and 37°C confirmed the increase in the aggregation

rate of nanoparticles in solution with temperature (Fig. 7b). The nanoparticle solution kept at 37 °C exhibited a higher secondary absorbance peak (caused by the formation of particle aggregates) at a wavelength around 960 nm and a more evident depletion of the primary absorbance peak (caused by the reduction of monodispersed nanoparticles in solution) when compared with the same solution kept at 23°C. As a result, at 37°C particle aggregates form at an increased rate and sediment faster than monodispersed nanoparticles in solution due their larger mass. Colloidal stability has been reported as one of the primary factors affecting the sedimentation–diffusion equilibrium of the nanoparticles [30].

The comparison between the sedimentation–diffusion behaviour of oppositely charged 100 nm gold nanoparticles in water at 23°C is shown in figure 8a. There are no evident deviations of the sedimentation rate exhibited by both types of nanoparticles tested but positively charged nanoparticles exhibit a higher concentration of not settled particles with respect to their negatively charged counterpart at equilibrium. This behaviour can be explained by considering the colloidal stability of the positively charged nanoparticles solution. The UV-Visible analysis (Fig. 8b) confirmed the presence of less aggregates in solution at 23°C after 4h when compared to the solution of negatively charged nanoparticles kept at the same temperature for the same time (i.e. no secondary absorption peak at longer wavelengths). Hence, more monodispersed particles are free to diffuse back into solution from the sediment leading to a higher concentration of not settled nanoparticles at equilibrium.

Nanoparticle sedimentation – diffusion equilibrium in biological solutions

To characterise nanoparticle behaviour in biologically-relevant solutions, the dynamics of sedimentation–diffusion equilibrium has been investigated by dispersing 100 nm diameter negatively-charged gold nanoparticles in Dulbecco's Modified Eagle Medium (DMEM) with 10% Fetal Bovine Serum (FBS). This solution was chosen because it is commonly used to support the growth of a range of mammalian cells. Figure 9 shows the absence of significant deviations between the settling dynamics of nanoparticles in DMEM with 10%FBS and in water at the same temperatures. This result, although interesting, is not surprising. So far, two of the main factors affecting the settling behaviour of nanoparticles have been inter-particle interactions and colloidal stability. The protein corona formed on the particle surface once they are dispersed in the biological solution prevents nanoparticle

aggregation otherwise induced by the high content of salts in solution and the temperature [31]. Moreover, the resultant complex gold-protein nanoparticles exhibit a zeta potential similar to the zeta potential of the same bare nanoparticles in water, between -20 mV and -40 mV [32, 33], meaning that the electrostatic interactions between the particles in water and DMEM+10%FBS have comparable magnitudes.

The dynamic viscosity of DMEM with 10%FBS has been reported to be just 5% higher than the dynamic viscosity of pure water [34], which is not enough to have a significant impact on nanoparticle kinetics [23].

Conclusion

In this paper, we have presented an experimental investigation of the process of achieving sedimentation-diffusion equilibrium for nanoparticles in solution and developed a theoretical model able to predict the settling dynamics of nanoparticles over time. The experimental results acquired demonstrate that nanoparticle size, colloidal stability and solution temperature drive the sedimentation-diffusion equilibrium of nanoparticles in solution and that, for particles larger than 60 nm in diameter, the target dose differs significantly from the administered dose in both water and cell culture medium. This evidence should be taken into account when performing in vitro studies using adherent 2D cultures, where the actual concentration of nanoparticles interacting with cells is needed to characterise and evaluate the cellular response. The theoretical model presented in this work shows good agreement with experimental data and is able to accurately describe the settling dynamics and concentration profile of nanoparticles in solution, making it a promising tool for the design of in vitro experiments and the study of concentration-response relationships.

Materials and methods

Experimental

Spherical negatively charged gold nanoparticles were purchased from BBI Solutions, with nominal diameters of 60 nm, 80 nm, 100 nm and 150 nm. Spherical positively charged gold nanoparticles were purchased from nanoComposix, with a nominal diameter of 100 nm. The as-supplied concentrations were reduced by adding the concentrate to deionised water as appropriate to obtain a constant working concentration of 5 x 108 particles ml−1. Nanoparticle dynamics in solution were

monitored in a standard optical inverted microscope (Axio Observer.Z1 m, Carl Zeiss) mounted on antivibration feet (VIBe, Newport) to isolate the sample from the environment. The microscope had been equipped with a stage-top incubation system (Incubator PM S1, Heating Insert P S1, Temp and CO2 module S1, Carl Zeiss) to control the temperature and the amount of CO2 present during the experiments. To generate caustic signatures of the nanoparticles some simple adjustments to the normal set up of the microscope were made following the procedure described by Patterson and Whelan [25]. The caustic curves generated are several orders of magnitude larger than the real nanoparticles in solution, allowing their detection in an optical microscope without any requirement for fluorescent labelling (Fig. S-1a in the Electronic Supplementary Material). The concentration profiles of the nanoparticles in solution were evaluated by acquiring z-stacks from the bottom to the top of the solution. The distance between consecutive images was set equal to 5 μm for a total acquisition length of 250 μm. The number of particles in each image was counted using the software ImageJ and integrated from the mid-depth (125 μm from the bottom) to the top (250 μm from the bottom) of the solution to obtain the total number of nanoparticles not settled at each time step (Fig. S-1b in the Electronic Supplementary Material). The depth of 125 μm was chosen because experimental observations demonstrated that particles formed a sediment that extended over the bottom half of the solution. Four solutions were prepared separately for each sedimentation test so that the results presented are average values with standard deviations. Each test was started 5 minutes after the injection of nanoparticles into the solution, to guarantee consistency between experiments and to allow nanoparticles to uniformly and randomly distribute throughout the medium. The concentration of nanoparticles not settled has been normalised so that the data presented are in the range 0 – 1. The settling time of each nanoparticle solution was established by evaluating the time at which the gradient of concentration of nanoparticles not settled over time was less than 5%.

Mason-Weaver equation

The objective in predictive analysis was to calculate the height profile of the nanoparticle concentration in the solution as a function of time. It was achieved by solving the Mason-Weaver convection-diffusion differential equation [19]:

$$\frac{\partial n(z,t)}{\partial t} = D\frac{\partial^2 n(z,t)}{\partial z^2} - V\frac{\partial n(z,t)}{\partial z} \qquad (1)$$

where *n(z,t)* is the normalized nanoparticle concentration, *D* is the diffusion coefficient and *V* is the sedimentation velocity (in our coordination system the sedimentation velocity is opposite to the *z*-axis orientation so *V*<0 in all equations). The initial condition was *n*=1 for all *z* and *t*=0. The boundary condition was based on an assumption of nanoparticle conservation in the system, expressed by no particle flux across the top and the bottom of the solution (at *z*=0 and *L* being the depth of the solution).

Giorgi-Macko model

Following the assumption that the diffusion coefficient *D* is not constant but depends on the local concentration of the nanoparticles and thus also on the position *z* and time *t*, the Mason-Weaver convection-diffusion differential equation in the form of (1) is not correct and needs to be derived supposing the function composition *D(n(z,t))*. We can start with the second Fick's law:

$$\frac{\partial n(z,t)}{\partial t} = -\frac{\partial J(z,t)}{\partial z} \tag{2}$$

where $J(z,t)$ is the flux of nanoparticles. In our scenario:

$$J(z,t) = J_D(z,t) + J_S(z,t) \tag{3}$$

where $J_D(z,t)$ is the diffusion flux defined by the first Fick's law:

$$J_D(z,t) = -D\big(n(z,t)\big)\frac{\partial n(z,t)}{\partial z} \tag{4}$$

and $J_S(z,t)$ is the sedimentation flux expressed as:

$$J_S(z,t) = Vn(z,t) \tag{5}$$

Combining (2) to (5) we get the Mason-Weaver equation with a non-constant *D:*

$$\frac{\partial n(z,t)}{\partial t} = \frac{\partial}{\partial z}\left(D(n(z,t))\frac{\partial n(z,t)}{\partial z}\right) - V\frac{\partial n(z,t)}{\partial z} \tag{6}$$

To solve it, the *z* coordinate was first transformed to a non-dimensional form:

$$z' = \frac{z}{L} \tag{7}$$

Then equation (6) was solved using the Euler explicit method where the derivatives were approximated by finite differences. The space and time domains were uniformly partitioned in a mesh. The space step was *L*/100 so the non-dimensional Δz = 0.01 and the time step Δt = 0.4s was chosen to maintain a stable solution of the equation over time.

The points $n(z_j', t_u) = n_j^u$ represent the numerical approximation of the concentration at the space point z_j' and time point t_u. The equation (6) after the approximation by finite differences becomes:

$$\frac{n_j^{u+1} - n_j^u}{\Delta t} = \frac{D(n_j^u)(n_{j+1}^u - n_j^u) - D(n_{j-1}^u)(n_j^u - n_{j-1}^u)}{L^2 \Delta z^2} - \frac{V(n_{j+1}^u - n_j^u)}{L \Delta z} \tag{8}$$

Using this relation and knowing the values of the concentration at time *u*, we can obtain the concentration at time *u+1* (computational stencil shown in figure 7):

$$n_j^{u+1} = n_j^u + \Delta t \left(\frac{D(n_j^u)(n_{j+1}^u - n_j^u) - D(n_{j-1}^u)(n_j^u - n_{j-1}^u)}{L^2 \Delta z^2} - \frac{V(n_{j+1}^u - n_j^u)}{L \Delta z} \right) \tag{9}$$

To calculate the nanoparticle concentration at the boundaries, we apply the boundary condition that there is no particle flux across the top and the bottom of the solution. By combining equations (2) and (3) the Mason-Weaver equation is obtained as function of the nanoparticle fluxes:

$$\frac{\partial n(z,t)}{\partial t} = -\frac{\partial}{\partial z}(J_D(z,t) + J_S(z,t)) \tag{10}$$

The derivatives in this equation (10) can be approximated by finite differences:

$$\frac{n_j^{u+1} - n_j^u}{\Delta t} = -\frac{1}{L}\frac{J_D'' - J_D'}{\Delta z} - \frac{1}{L}\frac{J_S'' - J_S'}{\Delta z} \tag{11}$$

where J_D'' and J_S'' are the diffusion and sedimentation fluxes between n_j^u and n_{j+1}^u, and J_D' and J_S' are the diffusion and sedimentation fluxes between n_{j-1}^u and n_j^u.

At the bottom boundary, z = 0 (*j* = 0), these four fluxes, depicted also in the computational stencil (Fig. 8), are as follows:

$$J_D^{\prime\prime} = -\frac{D(n_0^u)}{L}\frac{(n_1^u - n_0^u)}{\Delta z}, \qquad J_D^{\prime} = 0$$

$$J_S^{\prime\prime} = Vn_1^u, \qquad J_S^{\prime} = 0$$

Consequently, the equation (11) at the bottom boundary becomes:

$$n_0^{u+1} = n_0^u + \Delta t\left(\frac{D(n_0^u)}{L^2}\frac{(n_1^u - n_0^u)}{\Delta z^2} - \frac{V}{L}\frac{n_1^u}{\Delta z}\right) \tag{12}$$

Similarly, at the top boundary, z = *L* (*j* = 100), and the four fluxes J_D'', J_S'', J_D', and J_S' (Fig. 9) are as follows:

$$J_D^{\prime\prime} = 0, \qquad J_D^{\prime} = -\frac{D(n_{99}^u)}{L}\frac{(n_{100}^u - n_{99}^u)}{\Delta z}$$

$$J_S^{\prime\prime} = 0, \qquad J_S^{\prime} = Vn_{100}^u$$

Consequently, the equation (11) at the top boundary takes the form:

$$n_{100}^{u+1} = n_{100}^u + \Delta t\left(-\frac{D(n_{99}^u)}{L^2}\frac{(n_{100}^u - n_{99}^u)}{\Delta z^2} + \frac{V}{L}\frac{n_{100}^u}{\Delta z}\right) \tag{13}$$

The diffusion coefficient *D*(*n*) as a function of the normalised local concentration of the nanoparticles *n* can be expressed as:

$$D(n) = D_{exp} + \frac{(D_{StEin} - D_{exp})n^k}{n_{50}^k + n^k} \tag{14}$$

where D_{exp} = 5 * 10^{-13} m^2 s^{-1} is the experimental value of the diffusion coefficient measured at a low concentration of nanoparticles [23]. D_{StEin} is the diffusion coefficient according to Stokes–Einstein equation, n_{50} = 1.4 is the nanoparticle relative concentration at which the transition from the Stokes–Einstein diffusion mode to the low concentration diffusion mode happens, *k* = 20 is the slope of the transition (Fig. S-2 in the Electronic Supplementary Material).

Declarations

Ethical Approval and Consent to participate

Not applicable.

Consent for publication

All authors consent to the publication of the manuscript in Particle and Fibre Toxicology.

Availability of data and materials

All datasets used or analysed during the current study are available from the corresponding author on reasonable request.

Competing interests

The authors declare that they have no competing interests.

Funding

FG gratefully acknowledges funding from the UK Engineering and Physical Sciences Research Council in the form of a PhD studentship and funding from the European Commission Joint Research Centre (JRC) in the form of a traineeship.

Acknowledgment

Not applicable.

Authors' information

Affiliations

Faculty of Science and Engineering, University of Liverpool, Liverpool L69 3GH, United Kingdom.

European Commission, Joint Research Centre (JRC), Ispra 21027, Italy.

Contributions

FG conducted the experiments under the direct supervision of JMC & EAP. FG & PM developed the mathematical model. MW & AW contributed to the design of the study and interpretation of the results. FG prepared the first draft of the manuscript and all authors contributed to the production of the final version. All authors have given approval to the final version of the manuscript.

Corresponding author

Correspondence to Francesco Giorgi at francesco.giorgi@liverpool.ac.uk

References

[1] Marian, M.; Seghezzi, W. Novel Biopharmaceuticals: Pharmacokinetics, Pharmacodynamics, and Bioanalytics in *Nonclinical Development of Novel Biologics, Biosimilars, Vaccines and Specialty Biologics.* L.M. Plitnick, L.M.; Herzyk, D.J. Eds.; Academic Press: Cambridge, **2013**, 97-137.

[2] Hardman, J.G.; Limbird, L.E.; Gilman, A.G. *The Pharmacological Basis of Therapeutics*; MCGraw-Hill: New York, **2001**.

[3] Cui, J.; Faria, M.; Björnmalm, M.; Ju, Y.; Suma, T.; Gunawan, S.T.; Richardson, J.J.; Heidari, H.; Bals, S.; Crampin, E.J.; Caruso, F. *A Framework to Account for Sedimentation and Diffusion in Particle-Cell Interactions*. Langmuir, **2016**, 32(47), 12394-12402.

[4] Daraee, H.; Eatemadi, A.; Abbasi, E.; Aval, S.F.; Kouhi, M.; Akbarzadeh, A.. *Application of gold nanoparticles in biomedical and drug delivery*. Artif. Cells Nanomed. Biotechnol., **2016**, 44(1), 410-422.

[5] Wei, M.; Li, S.; Le, W. *Nanomaterials modulate stem cell differentiation: biological interaction and underlying mechanisms*. J. Nanobiotechnology. **2017**, 15(1), 75.

[6] Qin, H.; Zhu, C.; An, Z.; Jiang, Y.; Zhao, Y.; Wang, J.; Liu, X.; Hui, B.; Zhang, X.; Wang, Y. *Silver nanoparticles promote osteogenic differentiation of human urine-derived stem cells at noncytotoxic concentrations*. Int. J. Nanomed. **2014**, 9(1), 2469-78.

[7] Kohl, Y.; Gorjup, E.; Katsen-Globa, A.; Büchel, C.; Von Briesen, H.; Thielecke, H. *Effect of gold nanoparticles on adipogenic differentiation of human mesenchymal stem cells*. J. Nanopart.Res., **2011**, 13(12), 6789-6803.

[8] Rischitor, G.; Parracino, M.; La Spina, R.; Urbán, P.; Ojea-Jiménez, I.; Bellido, E.; Valsesia, A.; Gioria, S.; Capomaccio, R.; Kinsner-Ovaskainen, A.; Gilliland, D.; Rossi, F.; Colpo, P.. *Quantification*

of the cellular dose and characterization of nanoparticle transport during in vitro testing. Part. Fibre Toxicol., **2016**, 13(1).

[9] Cho, E.C.; Zhang, Q.; Xia, Y. *The effect of sedimentation and diffusion on cellular uptake of gold nanoparticles*. Nat. Nanotechnol., **2011**, 6(6), 385-391

[10] Hinderliter, P. M.; Minard, K. R.; Orr, G.; Chrisler, W. B.; Thrall, B. D.; Pounds, J. G.; Teeguarden, J.G. *Isdd: a computational model of particle sedimentation, diffusion and target cell dosimetry for in vitro toxicity studies*. Part. Fibre Toxicol., **2010**, 7(36).

[11] Chang, Q. *Sedimentation in Colloid and interface chemistry for water quality control*. Chang, Q, Eds.; Academic Press: Cambridge, **2016**, 23-35.

[12] Zheng, X.; Li, Y.; Chen, D.; Zheng, A.; Que, Q. *Study on analysis and sedimentation of alumina nanoparticles*. Int. J. Environ. Res. Public Health, **2019**, 16(3).

[13] Alexander, C.M.; Dabrowiak, J.C.; Goodisman, J. *Gravitational sedimentation of gold nanoparticles*. J. Colloid Interface Sci., **2013**, 396, 53-62.

[14] Liu, Z.; Wang, C.; Hou, J.; Wang, P.; Miao, L.; Liv, B.; Yang, Y.; You, G.; Xu, Y.; Zhang, M.; Ci, H. *Aggregation, sedimentation, and dissolution of CuO and ZnO nanoparticles in five waters*. Environ. Sci. Pollut. Res., **2018**, 25(31), 31240-31249.

[15] Haiss, W.; Thanh, N.T.K.; Aveyard, J.; Fernig, D.G. *Determination of size and concentration of gold nanoparticles from UV-Vis spectra*. Anal. Chem., **2007**, 79(11), 4215-4221.

[16] Zuber, A.; Purdey, M.; Schartner, E.; Forbes, C.; van der Hoek, B.; Giles, D.; Abell, A.; Monro, T.; Ebendorff-Heidepriem, H. *Detection of gold nanoparticles with different sizes using absorption and fluorescence based method*. Sens. Actuators B Chem. **2016**, 227, 117-127.

[17] Hsiung, C.E.; Lien, H.L.; Galliano, A.E.; Yeh, C.S.; Shih, Y.H. *Effects of water chemistry on the destabilization and sedimentation of commercial TiO2 charge neutralization*. Chemosphere, **2016**, 151, 145-151.

[18] Johnston, S.T.; Faria, M.; Crampin, E.J. *An analytical approach for quantifying the influence of nanoparticle polydispersity on cellular delivered dose*. J. R. Soc. interface, **2018**, 15(144).

[19] Mason, M.; Weaver, W. *The settling of small particles in a fluid*. Phys. Rev., **1924**, 23(3), 412-426.

[20] Midelet, J.; El-Sagheer, A.H.; Brown, T.; Kanaras, A.G.; Werts, M.H.V. *The Sedimentation of Colloidal Nanoparticles in Solution and Its Study Using Quantitative Digital Photography*. Part. Part. Syst. Charact., **2017**, 34(10).

[21] Giorgi, F.; Coglitore, D.; Curran, J.M.; Gilliland, D.; Macko, P.; Whelan, M.; Worth, A.; Patterson, E.A. *The influence of inter-particle forces on diffusion at the nanoscale*. Sci. Rep., **2019**, 9(1).

[22] Tuteja, A.; Mackay, M.E.; Narayanan, S.; Asokan, S.; Wong, M.S. *Breakdown of the continuum Stokes-Einstein relation for nanoparticle diffusion*. Nano Lett., **2007**, 7(5), 1276-1281.

[23] Coglitore, D.; Edwardson, S.P.; Macko, P.; Patterson, E.A.; Whelan, M. *Transition from fractional to classical Stokes-Einstein behaviour in simple fluids*. R. Soc. Open Sci., **2017**, 4(12).

[24] Liyanage, D.D.; Thamali, R.J.K.A.; Kumbalatara, A.A.K.; Weliwita, J.A.; Witharana, S. *An Analysis of Nanoparticle Settling Times in Liquids*. J. Nanomater., **2016.**.

[25] Patterson, E.A.; Whelan, M.P. *Tracking nanoparticles in an optical microscope using caustics*. Nanotech., **2009**, 19(10).

[26] Ganguly, S.; Chakraborty, S. *Sedimentation of nanoparticles in nanoscale colloidal suspensions.* Phys. Lett. Sect. A Gen. At Solid State Phys., **2011**, 375(24), 2394-2399.

[27] Kourki, H.; Famili, M.H.N. *Particle sedimentation: Effect of polymer concentration on particle-particle interaction*. Powder. Technol., **2012**, 221, 137-143.

[28] Koenig, G.; Ong, R.; Cortes, A.; Moreno-Razo, J.; De Pablo, J.; Abbot, N. *Single nanoparticle tracking reveals influence of chemical functionality of nanoparticles on local ordering of liquid crystal and nanoparticle diffusion coefficients*. Nano Lett., **2009**, 9, 2794–2801.

[29] Dutta, A.; Paul, A.; Chattopadhyay, A. *The effect of temperature on the aggregation kinetics of partially bare gold nanoparticles*. RSC Adv., **2016**, 6(85), 82138-82149.

[30] Jiang, W.; Ding, G.; Peng, H.; Hu, H. *Modeling of nanoparticles' aggregation and sedimentation in nanofluid*. Curr. Appl. Phys., **2010**, 10(3), 934-941.

[31] Pamies, R.; Cifre, J.G.H.; Espín, V.F.; Collado-González, M.; Baños, F.G.D.; De La Torre, J.G. *Aggregation behaviour of gold nanoparticles in saline aqueous media*. J. Nanopart. Res., **2014**, 16(4).

[32] Piella, J.; Bastús, N.G.; Puntes, V. *Size-dependent protein-nanoparticle interactions in citrate-stabilized gold nanoparticles: The emergence of the protein corona*. Bioconjugate Chem., **2017**, 28(1), 88-97.

[33] Ehrenberg, M.S.; Friedman, A.E.; Finkelstein, J.N.; Oberdörster, G.; McGrath, J.L. *The influence of protein adsorption on nanoparticle association with cultured endothelial cells*. Biomaterials, **2009**, 30(4), 603-610.

[34] Fröhlich, E.; Bonstingl, G.; Höfler, A.; Meindl, C.; Leitinger, G.; Pieber, T.R.; Roblegg, E. *Comparison of two in vitro systems to assess cellular effects of nanoparticles-containing aerosols*. Toxicol. In Vitro., **2013**, 27(1), 409-41.

[35] Stylianopoulos, T.; Poh, M.Z.; Insin, N.; Bawendi, M.G.; Fukumura, D.; Munn, L.L.; Jain, R.K. *Diffusion of particles in the extracellular matrix: The effect of repulsive electrostatic interactions*. Biophys. J., **2010**, 99(5),1342-1349.

Supplementary material

The supplementary material associated with this paper is available free of charge on the BMC website. **Figure S1:** (a) Photograph of a caustic generated by a 100 nm diameter gold nanoparticle in solution and (b) typical image acquired during the experiment showing 100 nm gold nanoparticles in solution. **Figure S2:** The diffusion coefficient *D(n)* as a function of the normalised local concentration of the nanoparticles n**. Figure S3:** Sedimentation velocity values used in the Giorgi–Macko model.

Figures

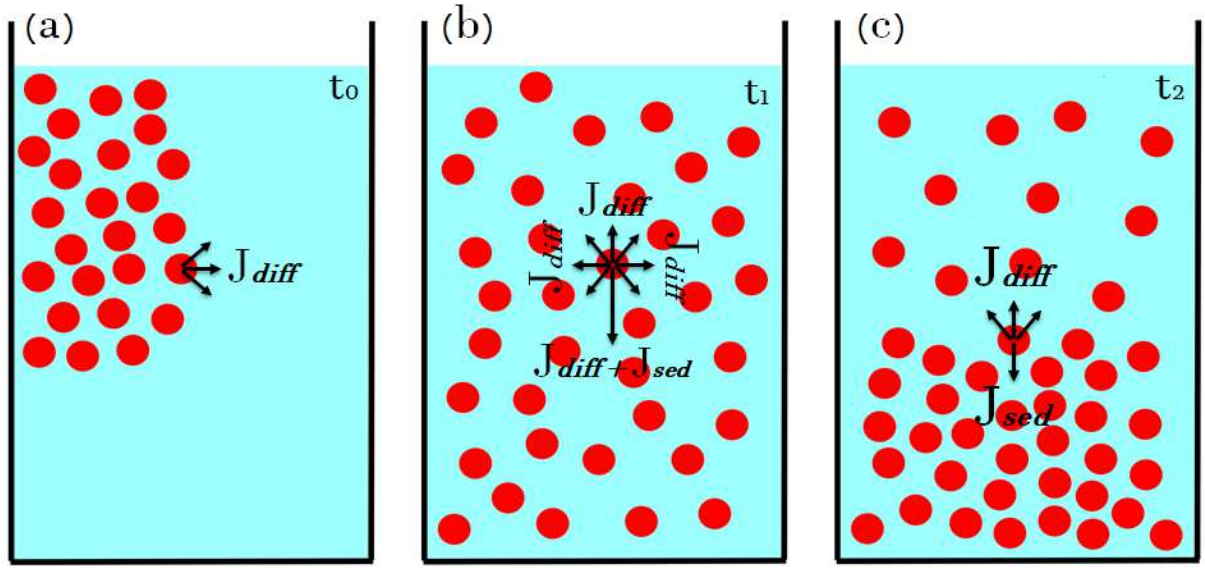

Figure 1: Schematics of the three steps of sedimentation-diffusion equilibrium for nanoparticles in solution: (a) once injected in solution nanoparticle dynamics is mainly regulated by diffusion forces. Nanoparticles are dispersed over the entire available volume; (b) nanoparticles are randomly but homogeneously dispersed in solution. Gravity tends to direct particles to the bottom of the solution; (c) sedimentation–diffusion equilibrium is attained. The rate of transport of nanoparticles in any one direction due to sedimentation equals the rate of transport in the opposite direction due to diffusion.

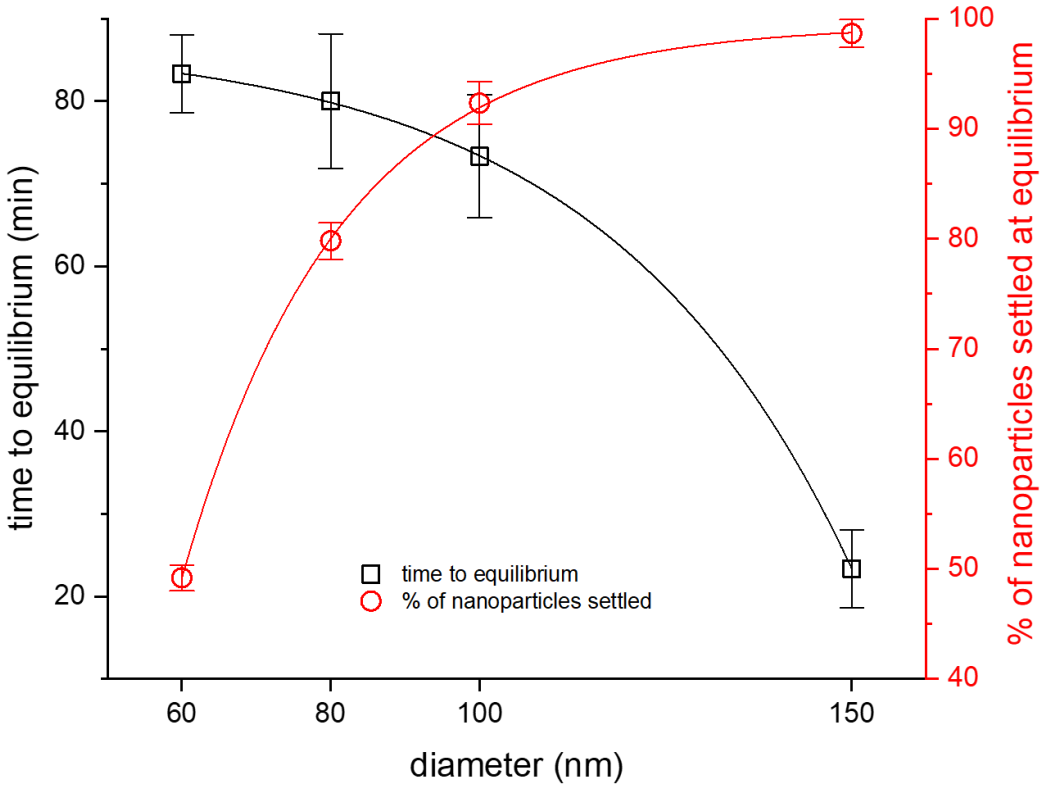

Figure 2: Experimental settling time (black squares and left axis) and percentage of nanoparticles settled at the equilibrium (red circles and right axis) as a function of nanoparticle diameters.

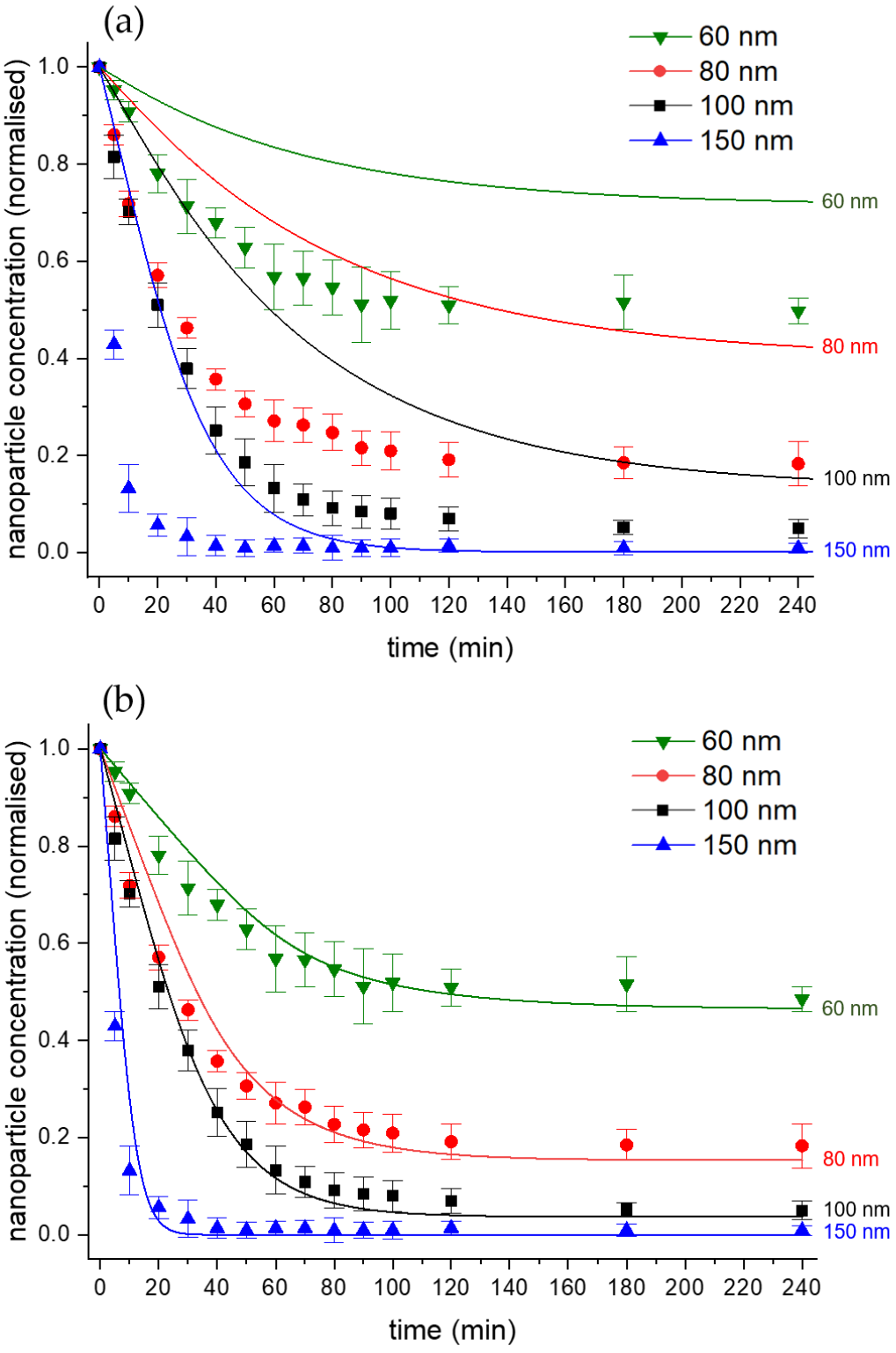

Figure 3: Measured concentration (symbols) of not-settled negatively-charged gold nanoparticles as a function of time in water at 23°C together with predictions (lines) from (a) the Mason–Weaver model and (b) the proposed modified Mason–Weaver model.

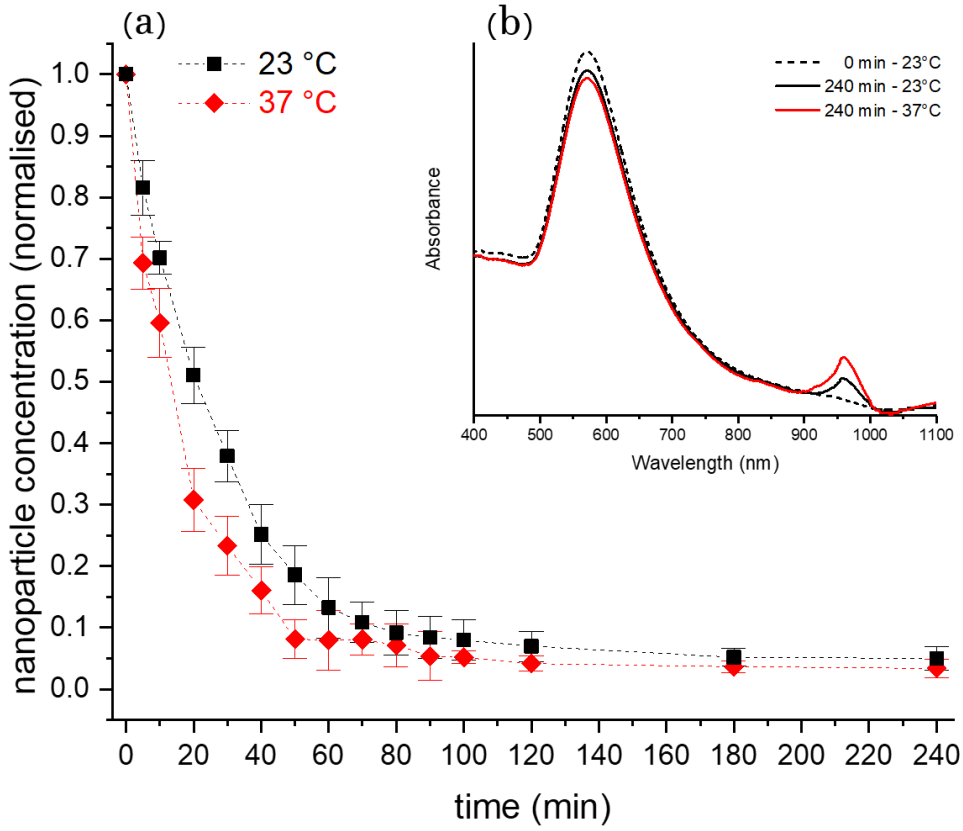

Figure 4: (a) Concentration of not-settled negatively-charged 100 nm diameter gold nanoparticles in water at 23°C (black squares) and 37°C (red rhombus) over time, and inset (b) UV-Visible absorption spectra of nanoparticle solutions at the beginning of the experiment (blue line) and after 240 minutes for solutions kept at 23°C (black line) and at 37°C (red line).

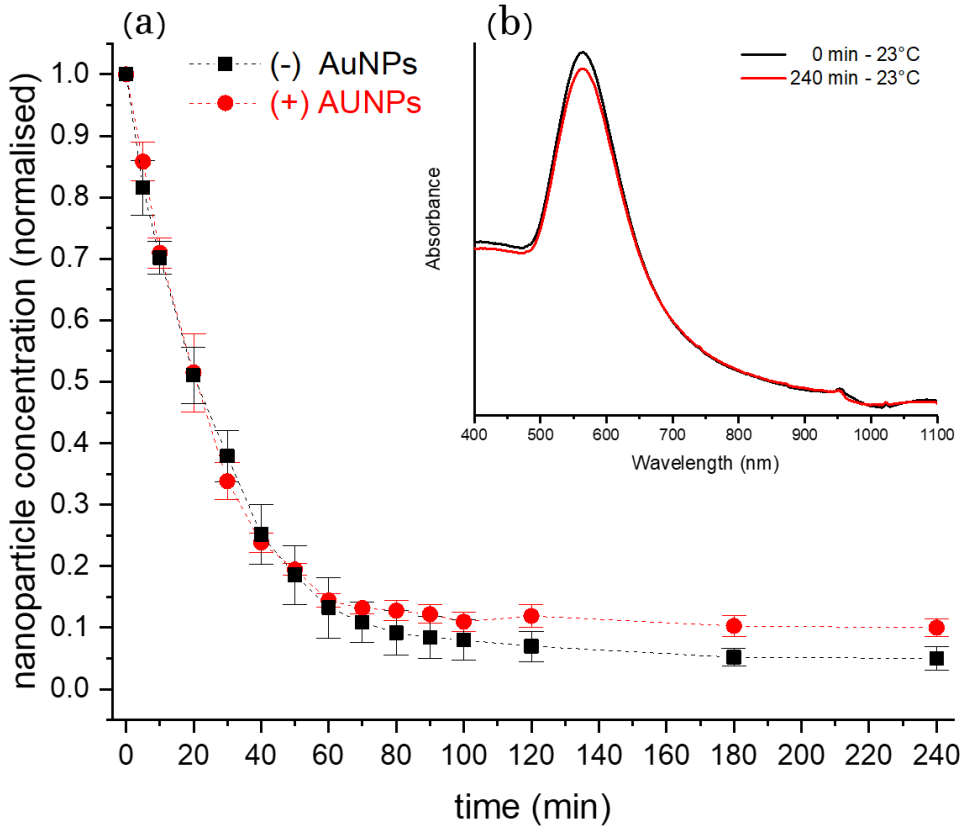

Figure 5: (a) Concentration of not-settled negatively charged (black squares) and positively-charged (red circles) 100 nm diameter gold nanoparticles in water at 23°C, and inset (b) UV-Visible absorption spectra of positively-charged nanoparticle solutions at the beginning of the experiment (black line) and after 240 minutes for solutions kept at 23°C (red line).

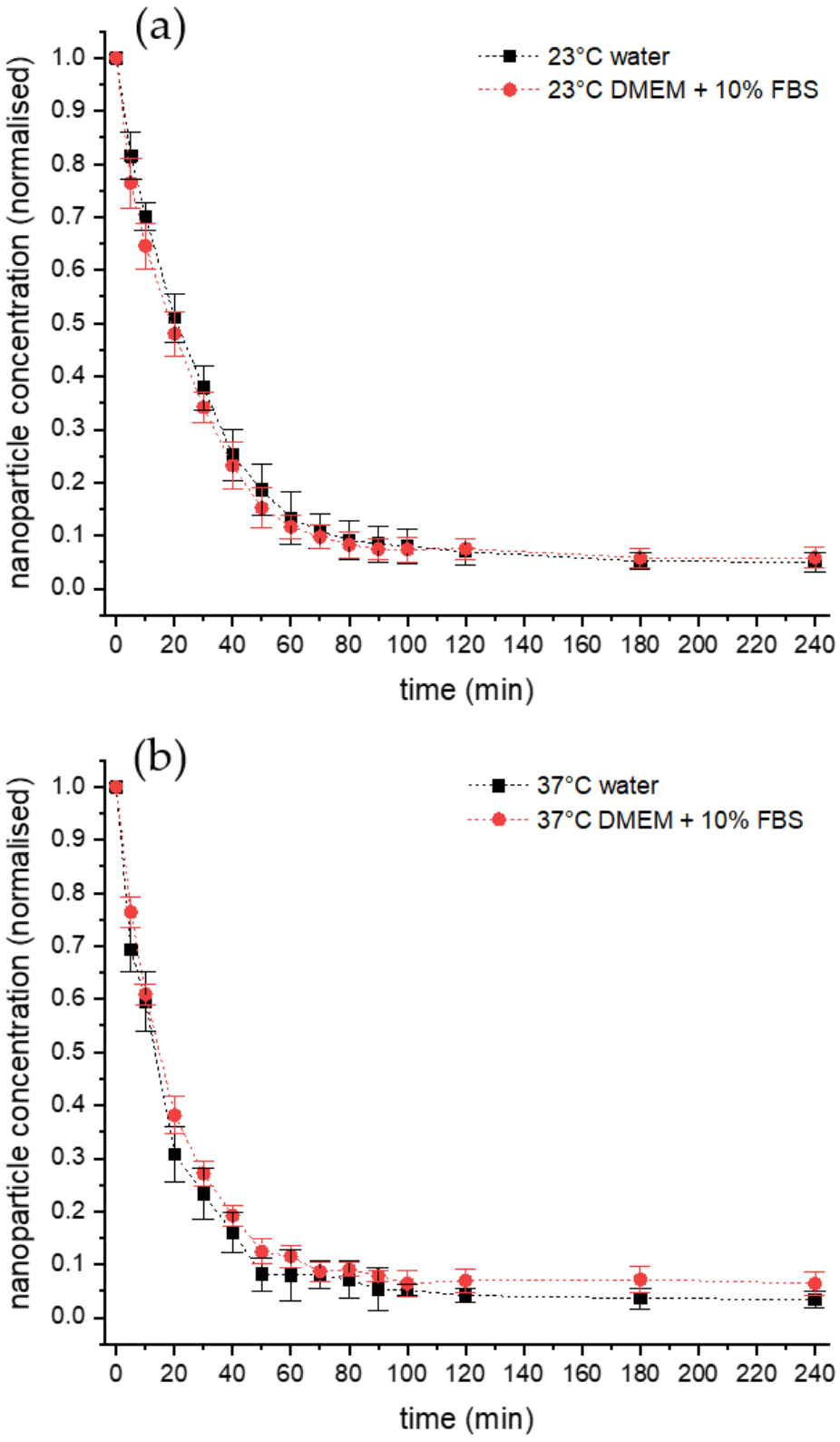

Figure 6: Concentration of not-settled negatively-charged 100 nm diameter gold nanoparticles in water (black squares) and in DMEM+10%FBS (red circle) as functions of time at 23°C (a) and 37°C (b)

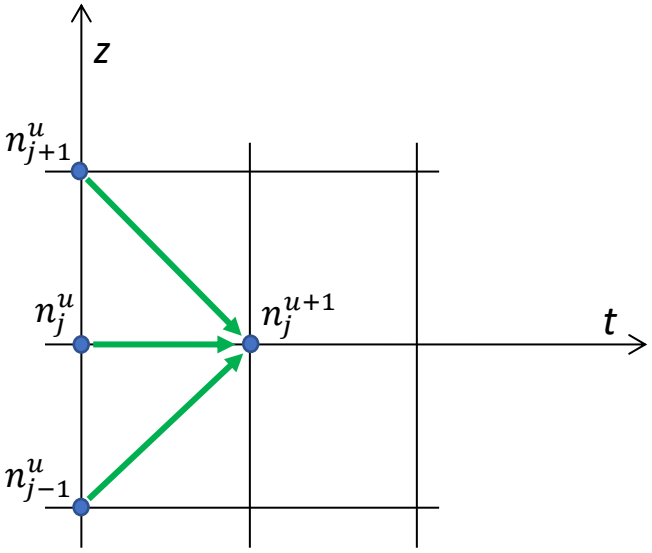

Figure 7: The difference computational stencil of the explicit Euler forward method.

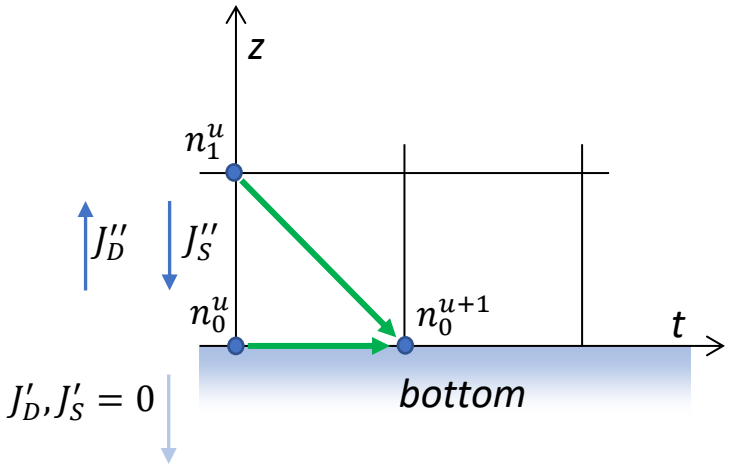

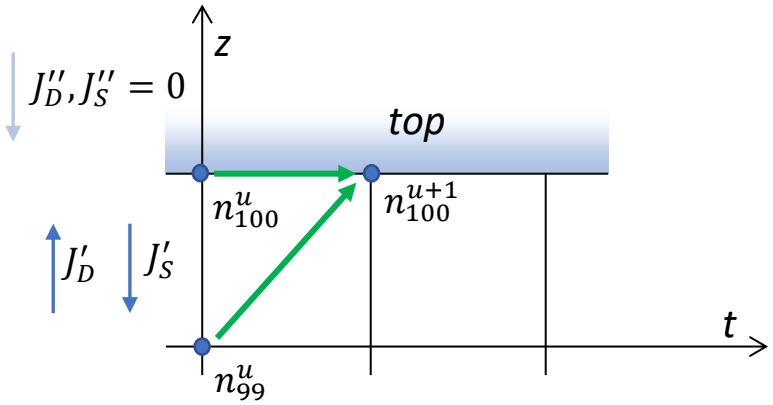

Figure 9: The difference computational stencil at the top with depicted fluxes.

Figures

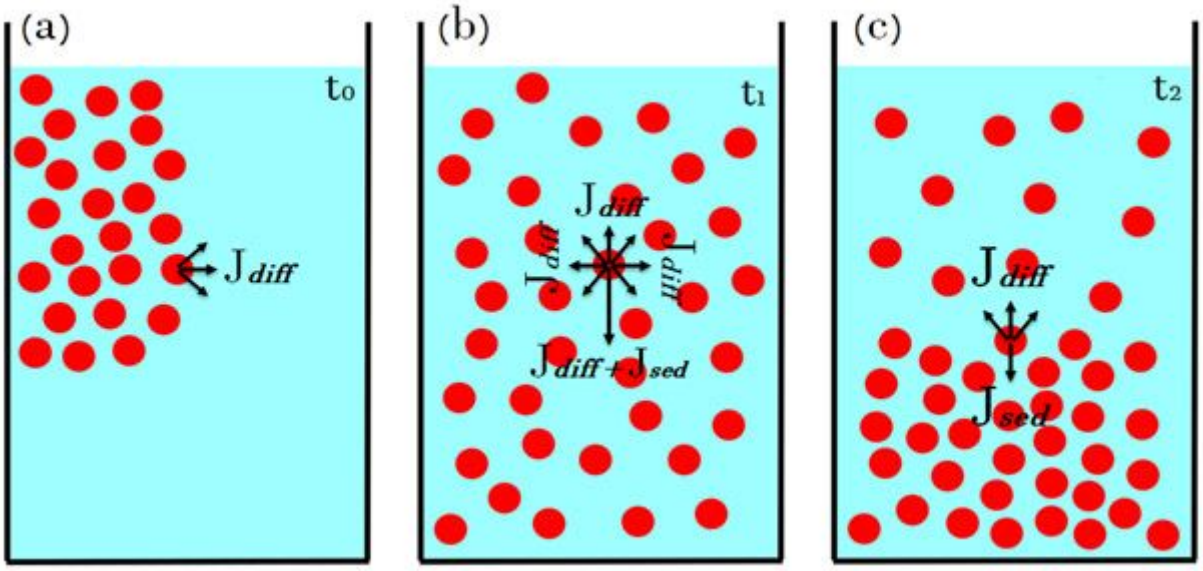

Figure 1

Schematics of the three steps of sedimentation-diffusion equilibrium for nanoparticles in solution: (a) once injected in solution nanoparticle dynamics is mainly regulated by diffusion forces. Nanoparticles are dispersed over the entire available volume; (b) nanoparticles are randomly but homogeneously dispersed in solution. Gravity tends to direct particles to the bottom of the solution; (c) sedimentation–diffusion equilibrium is attained. The rate of transport of nanoparticles in any one direction due to sedimentation equals the rate of transport in the opposite direction due to diffusion.

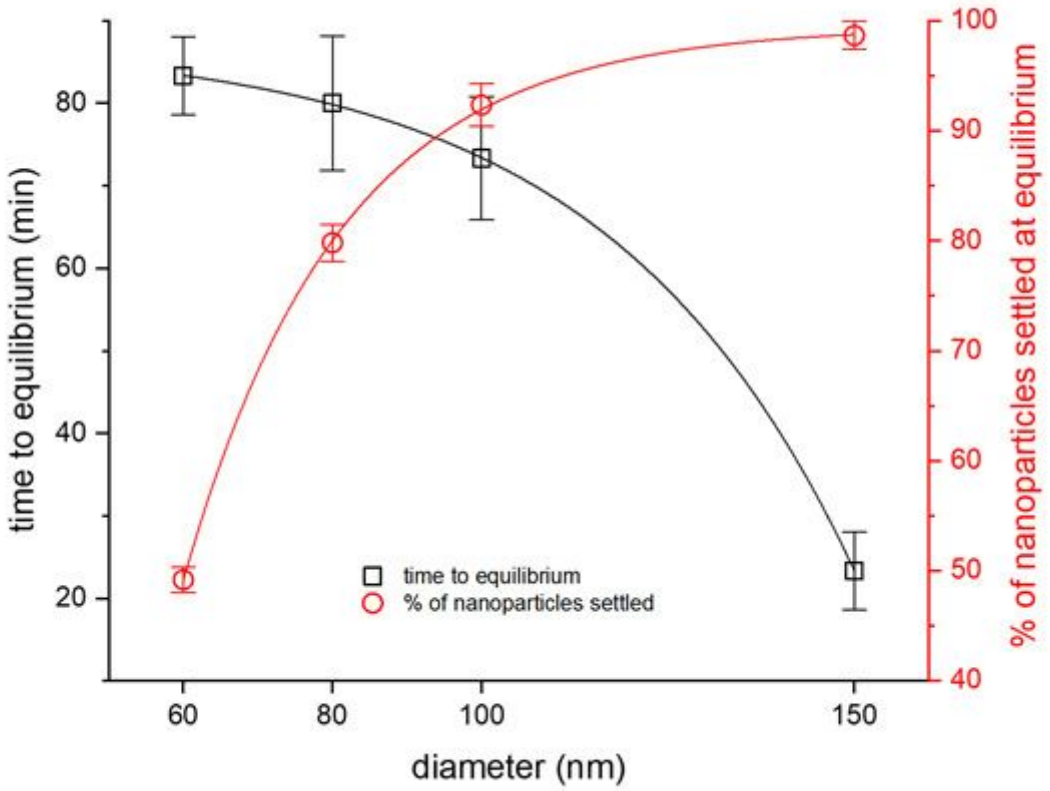

Figure 2

Experimental settling time (black squares and left axis) and percentage of nanoparticles settled at the equilibrium (red circles and right axis) as a function of nanoparticle diameters.

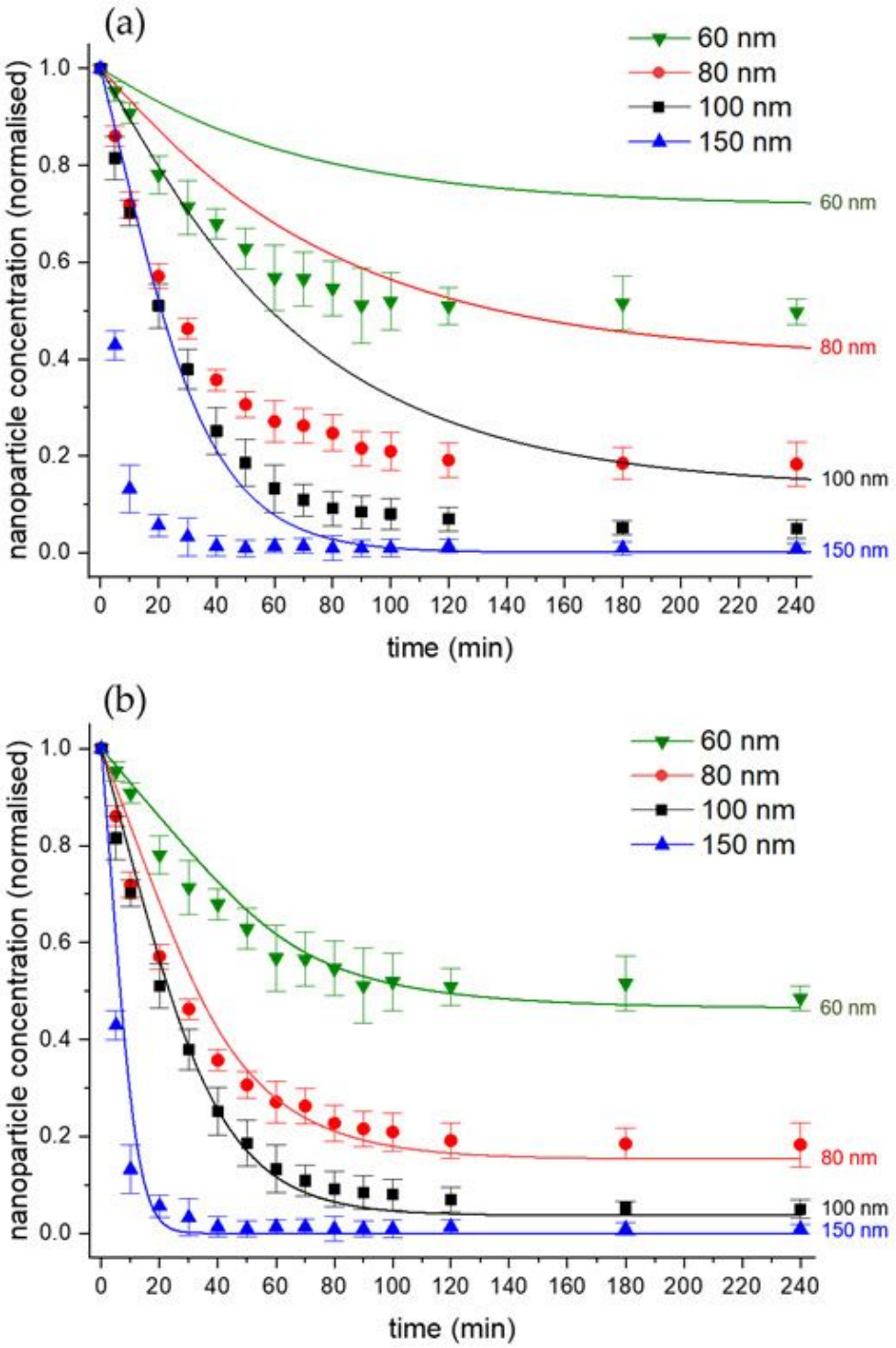

Figure 3

Measured concentration (symbols) of not-settled negatively-charged gold nanoparticles as a function of time in water at 23°C together with predictions (lines) from (a) the Mason–Weaver model and (b) the proposed modified Mason–Weaver model.

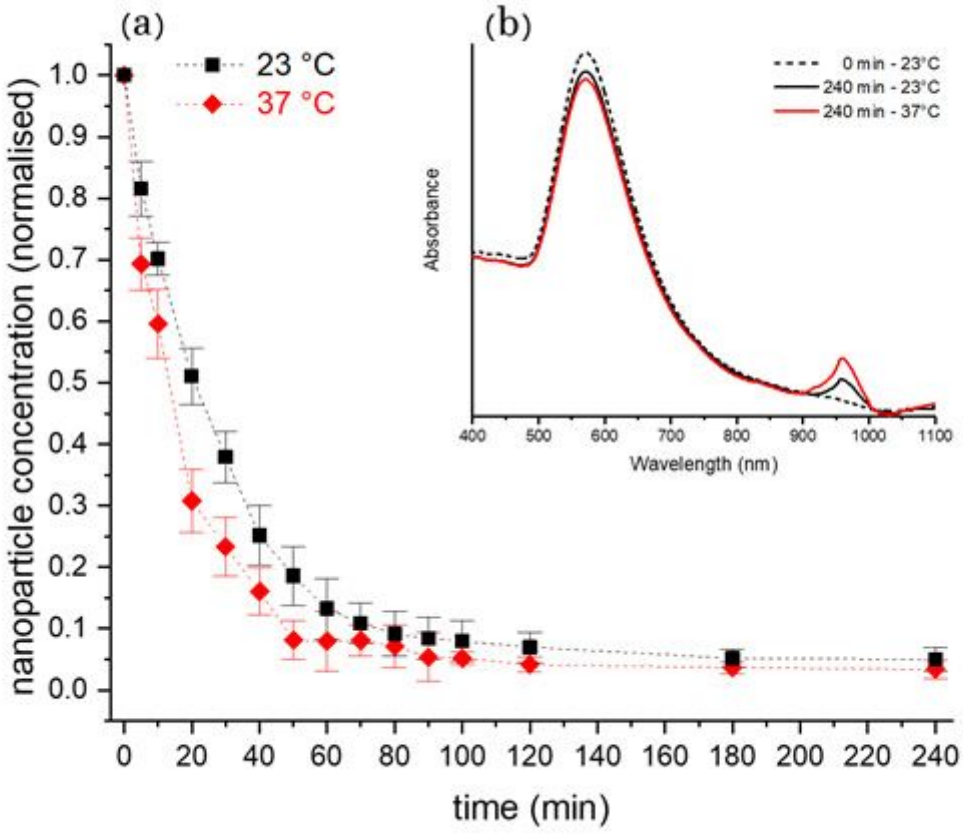

Figure 4

(a) Concentration of not-settled negatively-charged 100 nm diameter gold nanoparticles in water at 23°C (black squares) and 37°C (red rhombus) over time, and inset (b) UV-Visible absorption spectra of nanoparticle solutions at the beginning of the experiment (blue line) and after 240 minutes for solutions kept at 23°C (black line) and at 37°C (red line).

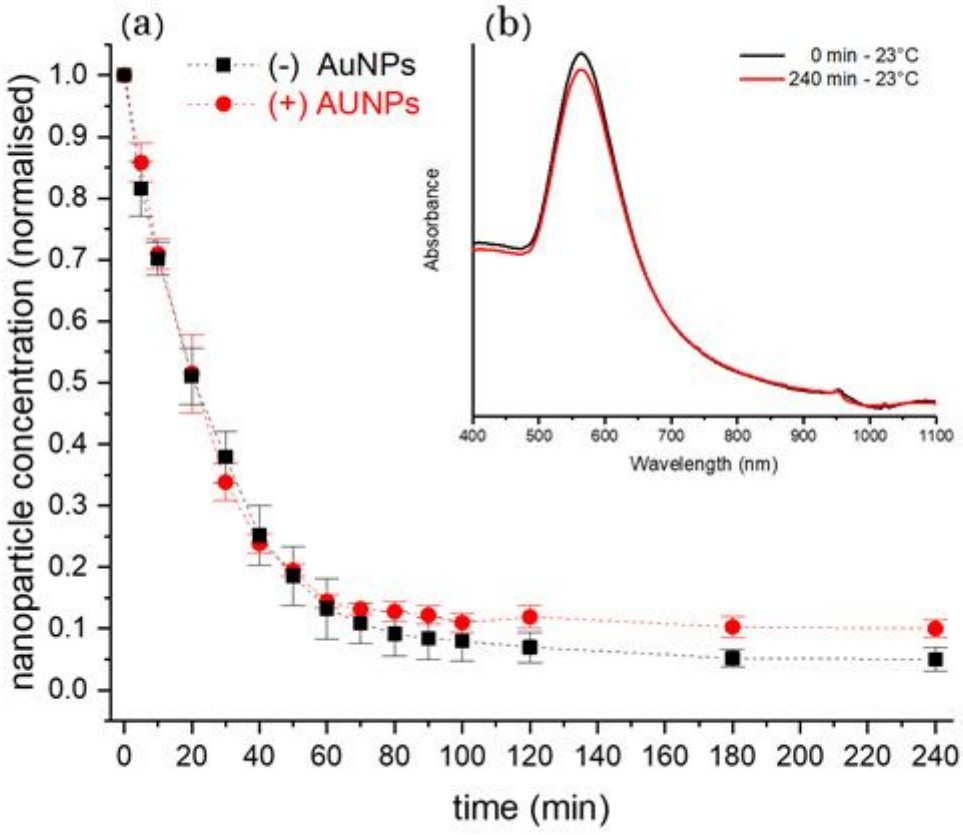

Figure 5

(a) Concentration of not-settled negatively charged (black squares) and positively-charged (red circles) 100 nm diameter gold nanoparticles in water at 23°C, and inset (b) UV-Visible absorption spectra of positively-charged nanoparticle solutions at the beginning of the experiment (black line) and after 240 minutes for solutions kept at 23°C (red line).

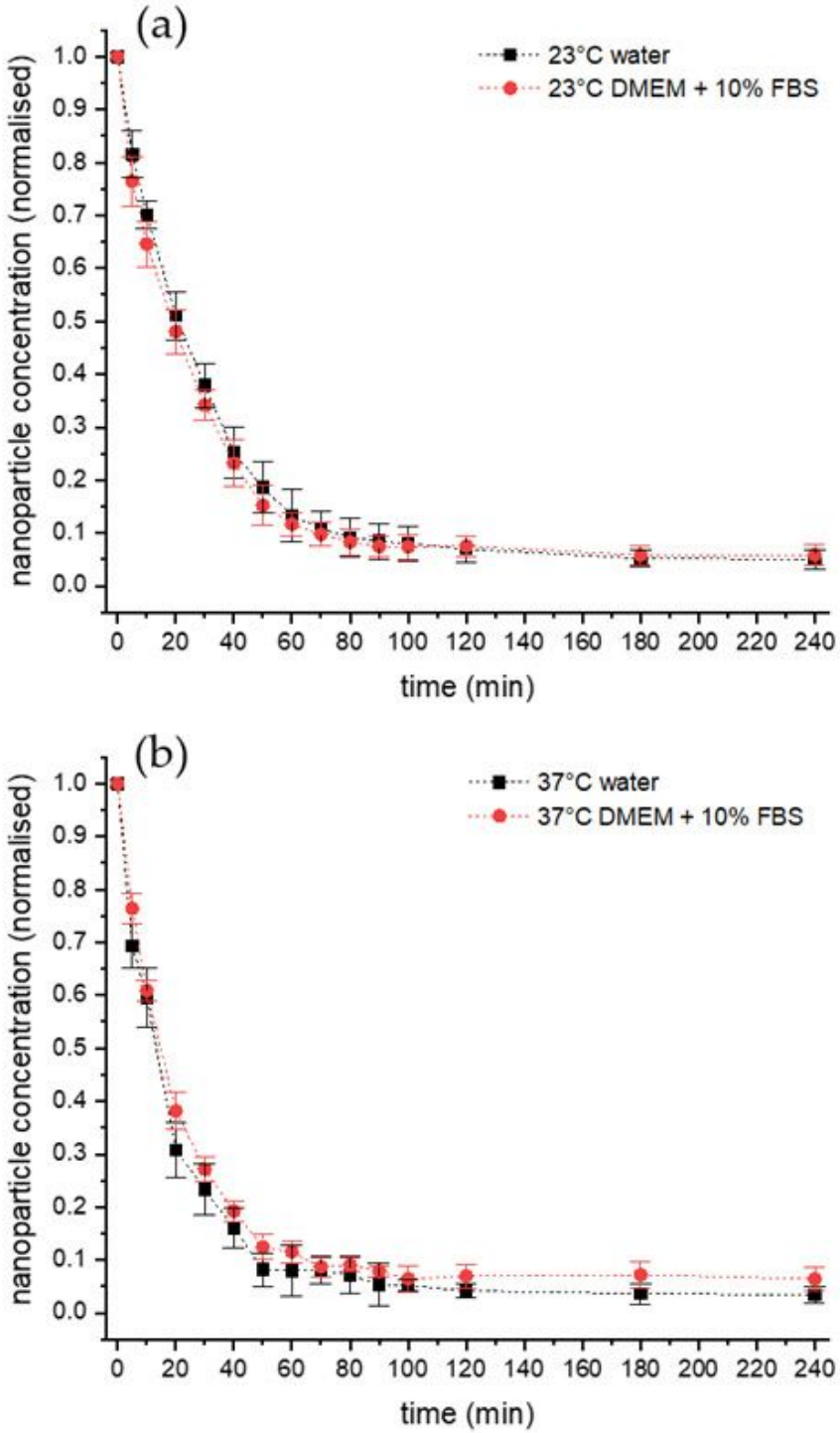

Figure 6

Concentration of not-settled negatively-charged 100 nm diameter gold nanoparticles in water (black squares) and in DMEM+10%FBS (red circle) as functions of time at 23°C (a) and 37°C (b)

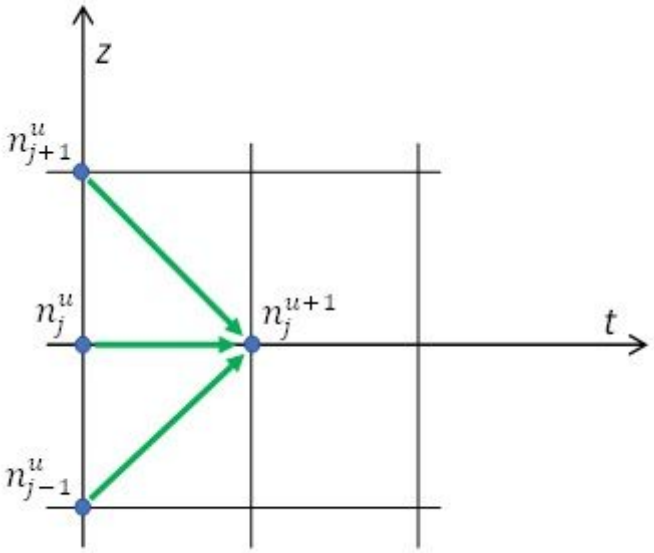

Figure 7

The difference computational stencil of the explicit Euler forward method.

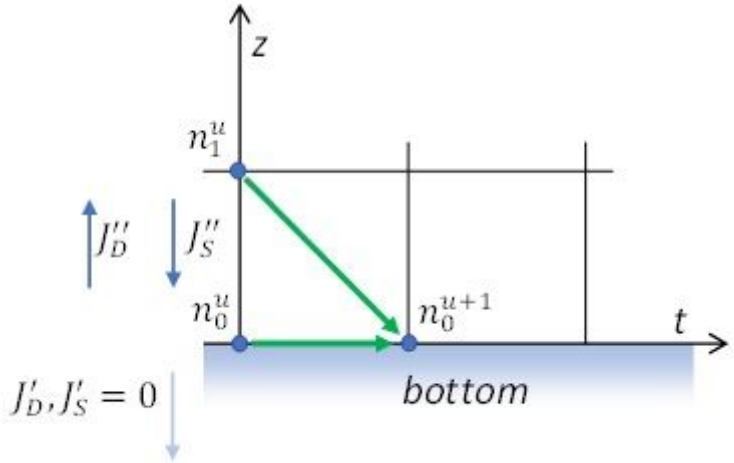

Figure 8

The difference computational stencil at the bottom with depicted fluxes.

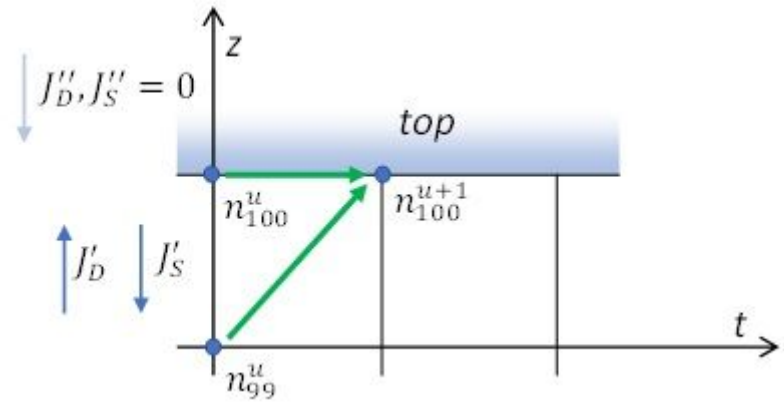

Figure 9

The difference computational stencil at the top with depicted fluxes.

Supplementary Files

This is a list of supplementary files associated with this preprint. Click to download.

- Supplementarymaterialsedimentationdiffusionbehaviour.docx
- Supplementarymaterialsedimentationdiffusionbehaviour.docx